Experimental study of shielding of propeller noise by a wing and comparison with model predictions

Alves Vieira, Ana; Malgoezar, Anwar; Snellen, Mirjam; Simons, Dick

Publication date
2018

Document Version
Accepted author manuscript

Published in
Euronoise 2018

Experimental study of shielding of propeller noise by a wing and comparison with model predictions

Ana Vieira, Anwar Malgoezar, Mirjam Snellen and Dick G. Simons
Section Aircraft Noise and Climate Effects, Faculty of Aerospace Engineering, Delft University of Technology, 2629 HS, Delft, The Netherlands.

Summary
The shielding of engine noise by the airframe of an aircraft is considered an effective way of reducing noise levels on the ground. Noise shielding in conventional aircraft is mainly due to the presence of the wings and most model predictions of full-scale aircraft neglect the effect of the airfoil curvature. The engine is typically simplified as a point source. The objective of such approximations is to reduce the complexity of the model implementation and to decrease the computational time. Measurements of noise shielding of a model wing took place in an anechoic facility using a microphone array. Two noise sources are considered: a point source and a model propeller. These measurements assess differences in noise shielding between using a point source and a source with strong directivity as a propeller. The comparison of experimental data with model predictions ascertain whether the simplifications commonly used in noise shielding problems are realistic. The noise shielding predictions use a method based on the Kirchhoff integral and the Modified Theory of Physical Optics (MTPO). This work aims to understand, using experimental data, possible limitations of noise shielding predictions when adopting typical simplifications.

1. Introduction

The high levels of annoyance associated with air traffic leads to resistance from part of the citizens regarding the expansion of the airports and to night curfews. This poses a problem considering the continuous growth of air traffic over the last decades and therefore, a considerable research effort is dedicated to reducing noise at the source and noise abatement operational procedures.

The awareness of the importance of reducing aircraft noise leads to innovative aircraft configurations such as the Blended Wing Body (BWB) [1] and distributed electric propulsion concepts [2]. These designs rely mostly on shielding of the engine noise by the airframe to reduce noise levels on ground.

Early predictions of shielding indicate high levels of engine noise reduction at the observers [3] and most results were validated using canonical cases with an exact solution. However, recent research supported by experimental data indicates lower values of noise shielding [4, 5]. Lower values of noise shielding than expected were also found by the analysis of flyover data of aircraft models with the engines mounted above the wing [6].

This work aims to understand the differences in noise shielding when using different noise sources and to compare experimental results with predictions. The shielding body considered in the experiments is a NACA wing and the sources considered are an omnidirectional customized source and a small propeller.

A microphone array is used to measure the individual sound pressure levels at the various microphone positions and to use beamforming techniques to reveal the source distribution on the shielding surface.

The predictions are based on the Kirchhoff integral theory and the Modified Theory of Physical Optics (MTPO) [7]. This method is accurate and fast enough to be included in the design optimization phase of an aircraft. Beamforming is also applied using the acoustic pressure values as calculated by the computational tool, which allows the comparison of the diffraction on the edges as found in the experiments and predictions.

The theoretical concepts used in this work are briefly explained in Section 2. Section 3 investigates the noise shielding of an omnidirectional source by a wing and compares the experimental data with predictions. In Section 4 the customized source is replaced by a propeller and the results in terms of noise shielding are compared to the results of Section 3. The

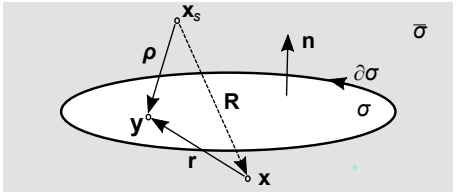

Figure 1. Kirchhoff integration across a circular aperture σ in the screen $\overline{\sigma}$.

main conclusions and future work recommendations are presented in Section 5.

2. Theory

2.1. Noise shielding calculation

The calculation of engine noise shielding in an aircraft is a challenging problem due to the complexity of the noise source and the medium conditions. Even the most common simplifications of considering the medium at rest and an omnidirectional source result in large computational times. In this work we use a method based on the Kirchhoff integral theory built on the Modified Theory of Physical Optics (MTPO). This method is a good trade-off between accuracy of the results and computational time, and can include sources with different directivity.

Consider an arbitrary aperture σ in a screen $\overline{\sigma}$, as represented in Fig. 1, between a source in position $\mathbf{x}_s$ and a receiver in position $\mathbf{x}$.

The scattered field p_s, and the field emitted by the source p_i, follow the Helmholtz equation in a volume of control that excludes the source location and the screen surface $\overline{\sigma}$. This system of equations can be rewritten by applying the Gauss-Green's theorem and using approximations on the boundary conditions to simplify the result. The scattered field is considered zero on the screen and it is approximated to zero far enough from the source. Also, p_s equals p_i in the aperture σ.

The pressure field at the receiver position $\mathbf{x}$ can be obtained by the calculation of the Kirchhoff integral over the aperture σ,

$$p_s^{aperture} = \frac{1}{4\pi}\int_\sigma \left[p_i \mathbf{n}\cdot\nabla\frac{e^{ik|\mathbf{r}|}}{|\mathbf{r}|} - \frac{e^{ik|\mathbf{r}|}}{|\mathbf{r}|}\mathbf{n}\cdot\nabla p_i\right] dS, \quad (1)$$

where $\mathbf{r} = \mathbf{y} - \mathbf{x}$, $\mathbf{y}$ is a position at the aperture and k is the wavenumber.

Evaluating the surface integral of Eq.1 is computationally demanding. So it is simplified using the theory of diffracted waves. This theory states that the scattered field is given by the undisturbed incident field p_{GO} and the boundary diffracted field p_d,

$$p_s^{aperture} = p_{GO} + p_d. \quad (2)$$

Here $p_{GO} = p_i\chi$, where χ is a delta function equal to unity when the ray from source to receiver passes through the aperture σ and zero otherwise.

Miyamoto and Wolf [8, 9] derived an expression for the diffracted field written in terms of a line integral $\partial\sigma$, which contributes significantly to a decrease of computational time,

$$p_d = \frac{1}{4\pi}\oint_{\partial\sigma}\frac{e^{ik|\boldsymbol{\rho}|}}{|\boldsymbol{\rho}|}\frac{e^{ik|\mathbf{r}|}}{|\mathbf{r}|}\frac{(\boldsymbol{\rho}\times\mathbf{r})\cdot d\mathbf{s}}{|\boldsymbol{\rho}||\mathbf{r}| + \boldsymbol{\rho}\cdot\mathbf{r}}, \quad (3)$$

where $\boldsymbol{\rho} = \mathbf{y} - \mathbf{x}_s$.

This line integral can be discretized in straight line segments and rewritten as a Fourier integral. This integral is evaluated using the method of the stationary phase, and the theory of the diffraction [10] is introduced to deal with the resulting singularities.

Finally, in order to calculate the scattered field due to the presence of the shielding object, p_s^{object}, the obstacle is interchanged with the aperture in the screen, following Babinet's principle [11],

$$p_s^{object} = p_i - p_s^{aperture}. \quad (4)$$

Now that p_s^{object} is known we can define a way of assessing values of noise shielding. A common way of presenting the noise reduction due to shielding is based on a shielding factor ΔL_p, given by

$$\Delta L_p = -20\log_{10}\left|\frac{p_s^{object}}{p_i}\right|, \quad (5)$$

with p_s^{object} and p_i representing effective pressures.

2.2. Beamforming

In this work we measured the sound pressure levels using a microphone array, which means that the sound pressure levels are acquired over a range of different angles and can be used collectively to localize and quantify noise sources, a procedure known as beamforming. The set of microphone signals is given as the vector $\mathbf{p}(t) \in \mathbb{R}^{N\times 1}$, where N is the number of microphones. After transforming the signal to the frequency domain $\mathbf{p}(\omega)$, we can construct the so-called cross spectral matrix (CSM) as

$$\mathbf{C}(\omega) = \mathbb{E}\left[\mathbf{p}(\omega)\mathbf{p}^*(\omega)\right], \quad (6)$$

where $\mathbb{E}(\cdot)$ is the expectation operator and $(\cdot)^*$ the complex conjugate transpose.

The source powers, and thus the resultant beamformer output, for a given scan point $\mathbf{x}_t$ can then be given as

$$B(\mathbf{x}_t, \omega) = \mathbf{h}^*(\mathbf{x}_t)\mathbf{C}(\omega)\mathbf{h}(\mathbf{x}_t), \quad (7)$$

where $\mathbf{h}(\mathbf{x}_t) \in \mathbb{C}^{N\times 1}$ is the steering vector and contains the theoretical microphone array responses of

potential sources. For the steering vector we use Formulation III of [12]. For the n-th element this is given by

$$h_n = \frac{1}{r_{t,n} r_{t,0} \sum_{n=1}^{N} \left(1/r_{t,n}^2\right)} e^{-j\omega(r_{t,n}-r_{t,0})/c}, \quad (8)$$

where $r_{t,n} = |\mathbf{x}_t - \mathbf{x}_n|$ is the distance between the scan point and microphone n and $r_{t,0} = |\mathbf{x}_t - \mathbf{x}_0|$ the distance between the scan point and the centre of the array. c stands for the speed of sound.

Eq. (7) is known as Conventional Beamforming (CB). The general approach is to define a number of scan points and estimate the source powers for each point using Eq. (7). The Sound Pressure Level (SPL) value at the array centre $\mathbf{x}_0$ can then be found as

$$L_p(\mathbf{x}_t, \omega) = 20 \log_{10} \left(\frac{\sqrt{B(\mathbf{x}_t, \omega)}}{p_0} \right), \quad (9)$$

with $p_0 = 20$ μPa, the reference pressure.

The levels are often depicted as a source map and the grid points usually lie in a plane. For the resultant image, high levels indicate the presence of a source $\mathbf{x}_t = \mathbf{x}_s$, whereas low levels indicate a mismatch $\mathbf{x}_t \neq \mathbf{x}_s$.

In this work beamforming is performed using both the shielding model predictions and experimental data. To have a fair comparison, the shielding model predictions will be sampled in space at points where also the real microphones are situated.

3. Experimental Procedure

The microphone array used in the measurements is composed by 64 40PH CCP Free-field Array Microphones, disposed in a metal grid using the TU Delft Optimized Array distribution [13]. This configuration provides the best trade-off for the Main Lobe Width (MLW) and Maximum Side lobe Level (MSL) in beamforming.

The microphones are connected to a National Instruments data acquisition (DAQ) computer. The computer consisted of a NI PXIe-1085 rack and has five PXIe-4499 Sound and vibration data acquisition modules.

The sound pressure in each microphone was recorded using LabVIEW virtual instrument. The recording time was 60 s and the sampling frequency was 50 kHz. Butterworth filtering was applied for band-passing the signal for the frequency range of interest.

The first source used in this experiment (Fig. 2 a) is a customized Miniature Sound Source type QindW developed by Qsources. The source sound power is omnidirectional in the azimuthal plane and has a flat frequency response from approximately 500 Hz to 6.3 kHz when driven by white noise.

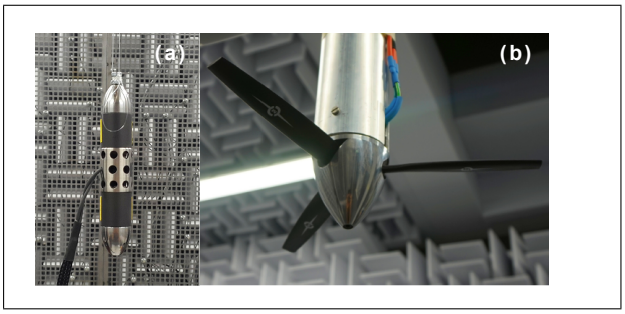

Figure 2. Sources used in the experiment: a) Onmidirectional source; b) Propeller.

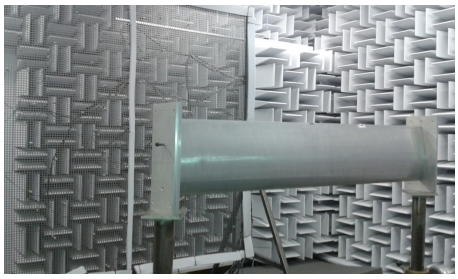

Figure 3. Wing used as shielding surface in the experiment.

The second source used is a 3-blade propeller Master Airscrew E-MA1260T (Fig. 2 b), connected to a Kontronik PYRO 700-45 Brushless motor. The motor is controlled with an electronic speed control (ESC) using a Kontronik Jive PRO 80+ HV.

The wing used as shielding surface has a chord of 24.5 cm and a length of 123 cm with an airfoil NACA 64-008A. The wing material is aluminium and it is supported by side plates and two metallic bars, as represented in Fig. 3.

The distances between the array and the sources and the array and the wing are varied in the experiments in order to have a large of amount of data for the comparisons. Due to the heavy structure necessary to fix the propeller, it is in a fixed position in the anechoic room and in this case only the wing was moved. Three different values of RPM were set for the propeller, corresponding to 50%, 80% and 87% of the motor's total capability.

4. Results

4.1. Noise shielding of an onmidirectional source

In this section we investigate the noise shielding of an omnidirectional source by a wing. A typical simplification in the calculations of engine noise shielding is considering the source as a monopole and the wings as flat plates. The latter simplification is considered realistic as the thickness of a wing is small when compared with the span. This means that only sharp-edge

diffracted rays are considered and the creeping rays (originating from smooth surfaces) are neglected.

In this first experiment we assess the differences between experiment and predictions for this particular case in terms of values for noise shielding. Beamforming is used to investigate the pattern of diffraction on the edges of the wing.

In this experiment nine different cases were considered, in which the relative distance between the source and the plate and the source and the array were varied. Considering that the array is composed of 64 microphones, this resulted in a very large dataset. Therefore, a way of condensing the results is to calculate the mean absolute deviation between experimental data and predictions, as indicated in Eq. 10

$$\delta = \frac{1}{N_{\text{sz}}} \sum_{N_{\text{sz}}} |\Delta L_{p,\text{prediction}} - \Delta L_{p,\text{experiment}}|, \tag{10}$$

where N_{sz} is the number of microphones in the zone where is expected shielding, i.e., the shadow zone.

Only the microphones in the shadow zone were considered, because it was verified that the levels microphones outside the shadow zone and therefore, without noise shielding, were correctly identified. If those microphones positions are taken into account in the mean absolute deviation, the value would decrease significantly and would no longer be representative.

The results of mean absolute deviation are represented as bar plots in Fig. 4, and the bars are placed in the corresponding d_{wing} (distance between the wing the source) and d_{array} (distance between the source and the array, i.e. the observers). Therefore, it is easy to observe to difference between experimental data and predictions, and to investigate if there is a correlation of the results with the position of the source relative to the wing or to the array.

Fig. 4 represents the mean absolute deviation between experimental data and predictions in terms of the Overall Sound Pressure Level (OSPL), and for the 1/3-Octave bands of 3150 Hz and 5000 Hz.

In terms of OSPL the mean absolute deviation between experimental results and predictions is around 3 dB.

To further investigate this, Fig. 5 represents the absolute difference between predictions and experimental data for each microphone in the array, in terms of OSPL, for the best and worst cases identified in Fig. 4 by green and red arrows, respectively. The negative values indicate overprediction of the computational tool and the values between light red and light green indicate a good agreement between predictions and experimental data (between 0 and -3 dB of difference).

Figs. 6 and 7 present the beamforming plots, for predictions and experimental data, for the best and worst cases of Fig.4, respectively. The frequency of 3150 Hz was selected for the best case and a frequency of 5000 Hz was selected for the worst one. The selected frequencies are different in order to have the best resolution in each case, since the distance of the array and the wing to the source are different in the two cases.

The beamforming plots of experimental data and predictions are very similar, although the experimental ones show less symmetry. This also helps explaining some of the differences between noise shielding. The experimental setup can be misaligned in relation to the observers and the analysis of the beamforming plots can be a useful tool to correct the position of the source relative to the shielding surface in the predictions and improve their accuracy.

4.2. Noise shielding of a propeller

In this section the source used in the experiment is a 3-blade propeller and the shielding surface is the same wing used in the previous section. The propeller is in a fixed position in the anechoic room because the support structure is attached to the nozzle of the wind tunnel in order to minimize vibrations caused by the high angular speed of the propeller.

The support structure of the propeller and the nozzle were covered with foam to avoid reflections. The nozzle is located in the middle of the anechoic room and therefore there is a limited space between the microphone array and the propeller to place the wing. Only two wing positions relative to the array (d_{wing}) were considered in this experiment, and the angular speed of the propeller was set at 50%, 80% and 87% of the motor's total capability. Table I displays the relative distances used in the experiment and the Blade Passage Frequencies(BPF) associated to motor's total capability percentages.

Unlike the customized source used in the previous section, the propeller is a complex source of noise, difficult to characterize and predict. The directivity of a propeller is typically associated to a dipole, however, different types of noise compose the overall propeller noise [14]. The displacement of the medium as the blades pass generates thickness noise (monopole nature), the loading on the blades is associated to loading noise and the interaction of the turbulent flow with the trailing edge of the blades generates trailing edge noise (quadrupole). Other sources of broadband noise as the interaction of tip vortices with the passing blade, for example, are also present.

In this experiment the propeller was operating under static conditions, which results in a non-uniform flow generated by the rotation of the propeller and therefore an increase of the unsteady loading noise [15]. However, it is not feasible to place both the wing and the propeller in the nozzle of the wind tunnel. The interaction between the wind tunnel inflow, the propeller wake and the absence of inflow around the plate could affect the noise shielding results. It is however a possible experiment to analyse in the future.

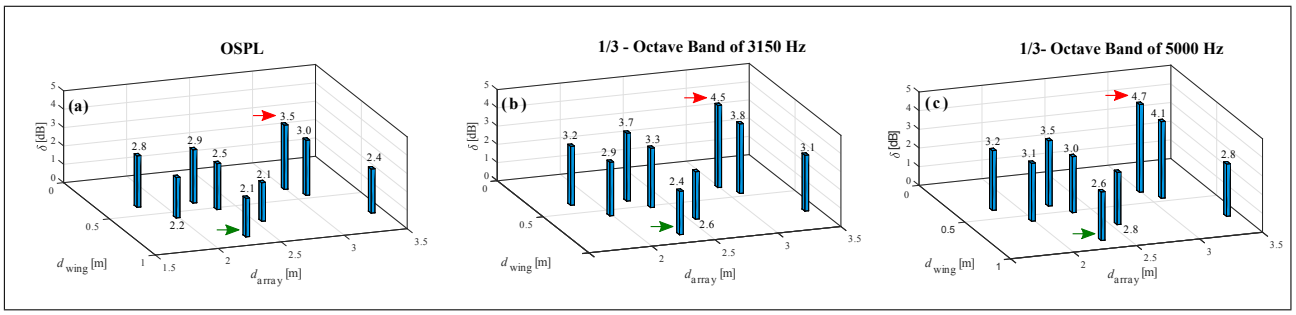

Figure 4. Average absolute deviation [dB] between experimental and computational results of noise shielding considering: a)OSPL; b) 1/3-Octave band of 3150 Hz; c)1/3-Octave band of 5000 Hz.

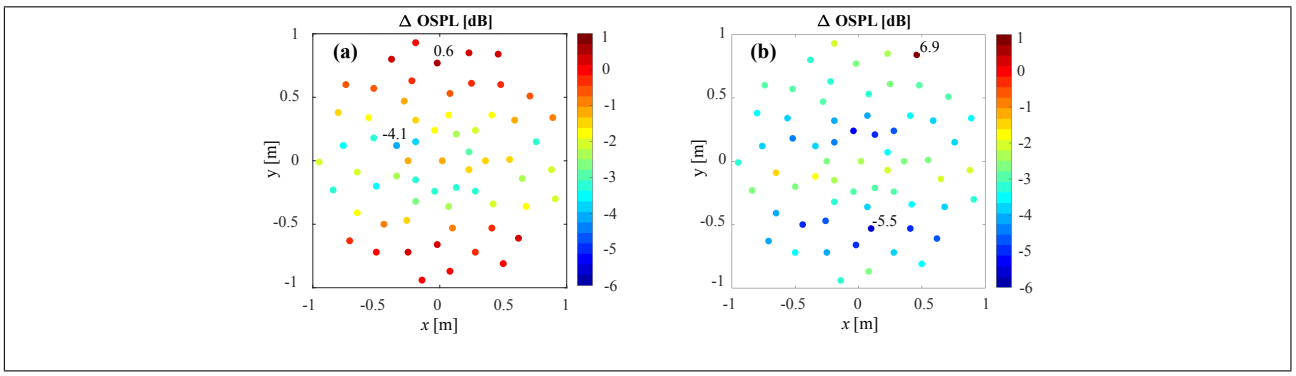

Figure 5. Absolute difference in each microphone in the array in terms of OSPL for: a) the best case, b) the worst case, of Fig. 4.

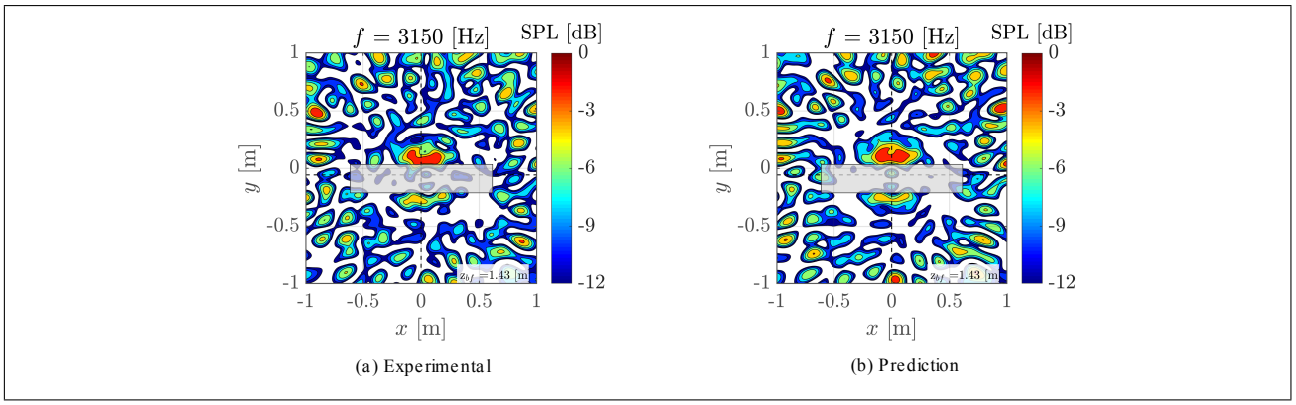

Figure 6. Beamforming plot at 3150 Hz for the best case of 4 a) experimental, b) prediction. The scale is in relation to the maximum value of SPL.

Table I. Distances considered in the experiment and Blade Passage Frequency (BPF) values of the propeller. d_{source} is the distance between the array and the source and d_{wing} is the distance between the array and the wing.

d_{source} [m]	1.46
d_{wing} [m]	1.07 0.90
BPF [Hz]	$\text{BPF}_1 = 220$ $\text{BPF}_2 = 350$ $\text{BPF}_3 = 380$

Firstly, the values of noise shielding in the microphone array found for the propeller at different values of angular speed are compared with an equivalent case considering the customized source (same distance d_{array} and d_{wing}). In Fig. 8 the values of noise shielding in the array, expressed in terms of OSPL, are illustrated for the customized source and the propeller at the three angular speeds considered in this experimental work.

The differences between the values of noise shielding considering the customized source and the propeller are evident. With the customized source the values of noise shielding are considerable (around -6 dB), whereas with the propeller the values of noise shield-

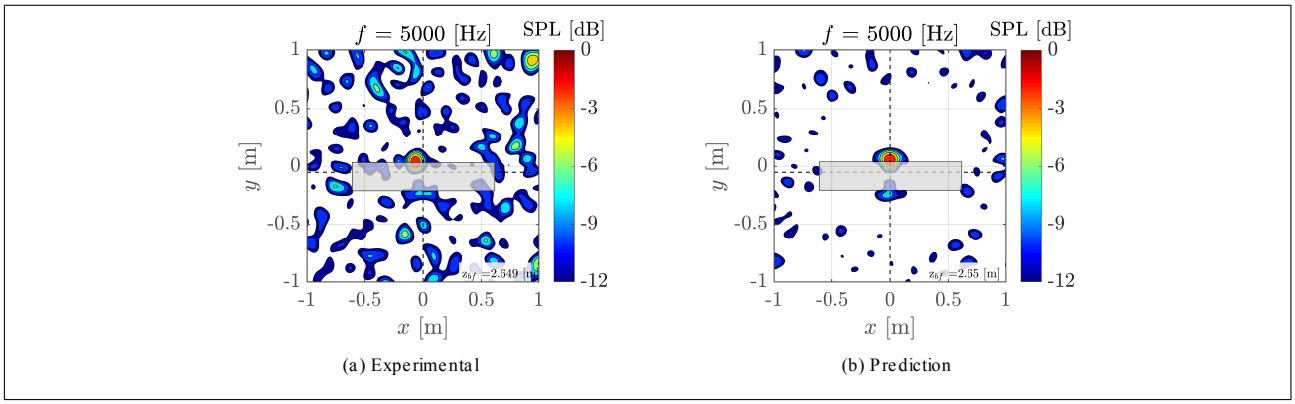

Figure 7. Beamforming plot at 5000 Hz for the worst case of 4: a) experimental, b) prediction. The scale is in relation to the maximum value of SPL.

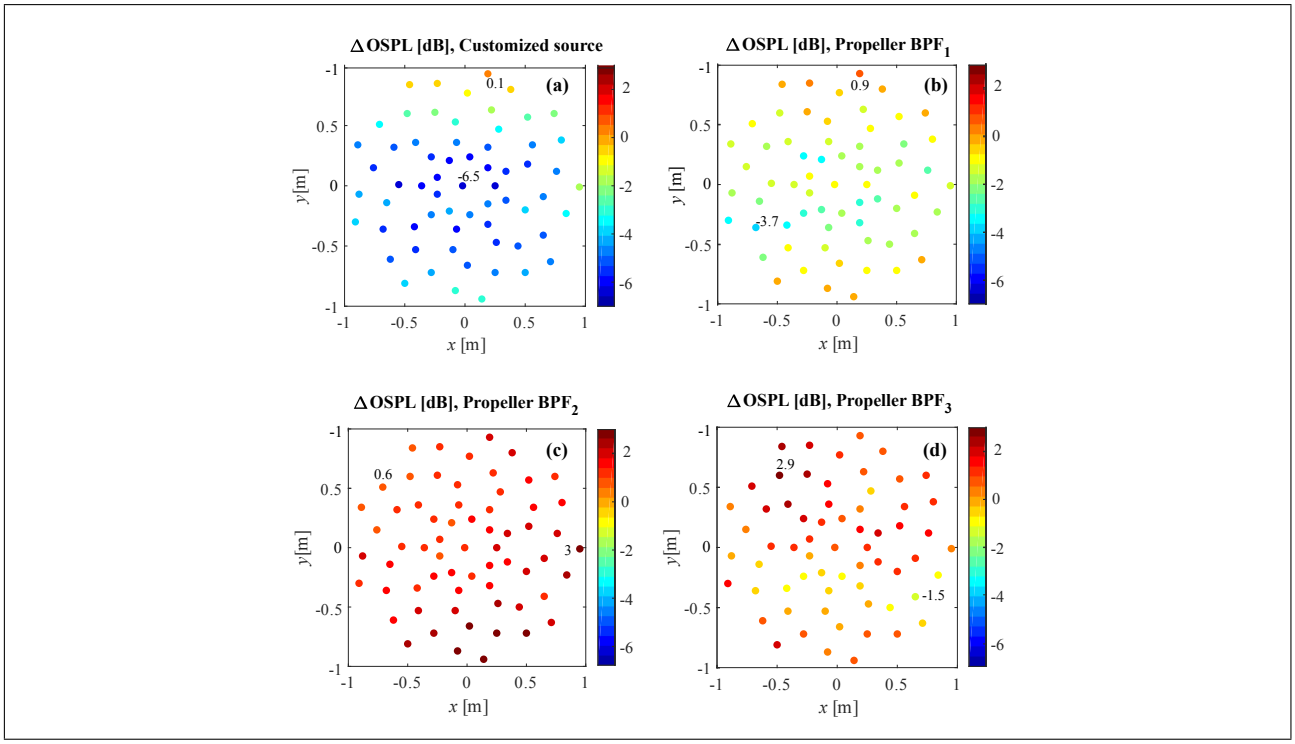

Figure 8. Experimental values of noise shielding expressed in OSPL for: a) Customized source, b) Propeller at BPF_1, c) Propeller at BPF_2, d) Propeller at BPF_3; $d_{wing} = 0.90$ m.

ing decrease abruptly for BPF_1 and are negligible for BPF_2 and BPF_3.

Although differences were expected due to the different nature of the noise source, an inexistence of noise shielding for the higher BPF values was not expected. An analysis of the noise spectrum of the experiments (Fig. 11 for BPF_1 and Fig. 12 for BPF_3) revealed that the majority of the peaks of the harmonics were not reduced by introducing the wing. The same was verified for the broadband noise. Other periodic sound sources besides the BPF frequencies of the propeller were identified in the spectrum. This result will be further investigated using beamforming.

Three frequencies of interest, indicated by black arrows, were selected from Fig. 9. These frequencies correspond to the 5th (1100 Hz) and 6th harmonic (1320 Hz) and a peak that stands out in the spectrum and does not correspond to a harmonic (at 2210 Hz). The

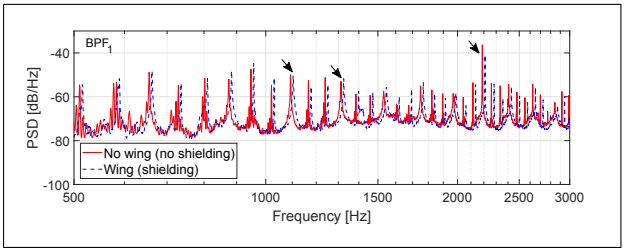

Figure 9. Power Spectral Density (PSD) for BPF_1 and d_{wing}=1.07 m.

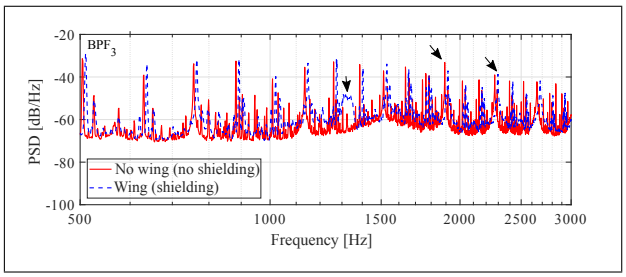

Figure 10. Power Spectral Density (PSD) for BPF_3 and d_{wing}=1.07 m.

BPF is slightly different in the experiments with and without the wing. The percentage of the motor's total capability was the same, however, only round numbers could be applied and therefore a small variation is expected.

In the 5th harmonic the peak of the spectrum with the wing is slightly lower than the peak of the spectrum without the wing, indicating noise shielding. On the contrary, the peak of the 6th harmonic is higher when the wing is present.

Observing Fig. 11 a), corresponding to the 5th harmonic, there are two sources distributed in the leading and trailing edges of the wing, as observed in the beamforming plots of the previous section, for the customized source. However, in the 6th harmonic, represented in Fig. 11 b), a third source appears in the top of the tube where the engine is placed. This other source explains why there is noise shielding for the 5th but not for the 6th harmonic. The peak around 2210 Hz, illustrated in Fig. 11 c), is associated to the noise of the electric motor since the source is located in the same position as the motor.

In the spectrum corresponding to BPF_3, of Fig. 10, other three frequencies were selected: the 5th and the 6th harmonics (corresponding to 1900 Hz and 2280 Hz, respectively) and a peak that only appears when the wing is introduced. Notice that the frequency corresponding to the motor is not a peak at this value of BPF.

In the 5th harmonic the peak of the spectrum with the wing is lower than when considering only the source, indicating noise shielding. Fig. 12 a) shows two sources in the leading and the trailing edges (indicating noise diffraction and therefore noise shielding) and a third small source which seems to be originated in the support. The 6th harmonic, however, seems to increase with the presence of the wing, and Fig. 12 b) only indicates one source at the trailing edge.

In Fig. 12 c) the sources are not only located in the support structure but also coming from a point of the anechoic room. There is no evidence of noise diffraction on the wing in this case. This was also observed for several other frequencies (not presented in this work) - sources coming from the support, nozzle, or from the anechoic room.

Noise shielding seems to occur only for the harmonics and not for broadband noise. The broadband noise seems to increase when the wing is present, which can be associated to the interaction between the turbulent flow and the wing surface.

5. CONCLUSIONS

In this work experiments were compared with predictions for the case of noise shielding of a customized source and a propeller by a NACA wing. Several distances and frequencies were analysed and a good agreement was found between experimental results and predictions for the case of the customized source. Beamforming was used to visualize the noise diffraction on the edges of the wing, using acoustic pressure values from experimental data and predictions. The beamforming plots are also useful to verify the relative position of the source and the shielding surface and to locate external noise sources in the experimental facility.

Although considering a monopole source is a common approach in shielding of engine noise, in reality the nature of engine noise is much more complex. The customized source was replaced by a 3-blade propeller in a second experiment. The noise shielding values found in this experiment were very low compared with the experiment considering the omnidirectional source.

The beamforming plots showed diffraction on the edges only for the harmonics and several external sources coming from the support structure, the electric motor and the anechoic room. Therefore, the propeller has a strong interaction with the surrounding structures originating new sources which eclipse the noise reduction due to shielding.

More research is needed to clarify and eliminate the origin of the new noise sources. The experiment can be repeated with the propeller at a constant axial inflow to assess differences in terms of noise shielding. Beamforming should be used to identify noise sources.

Many new low-noise aircraft designs rely on noise shielding to reduce noise on ground. Most analyses consider sources with simple directivity patterns such as monopoles or dipoles. The experiments discussed in this work show that noise shielding is strongly dependant on the noise source and therefore more work should be performed on this topic.

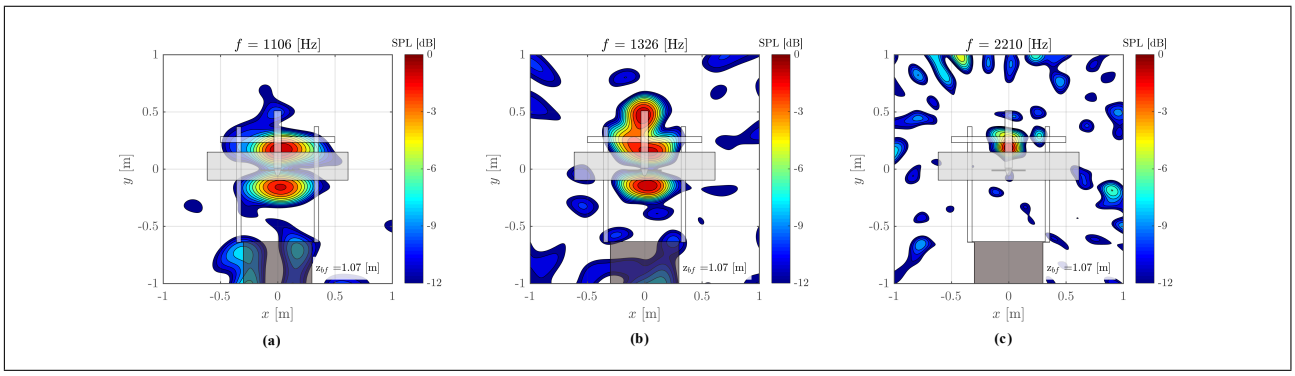

Figure 11. Beamforming for the propeller at the angular speed of BPF_1, for a frequency of: a) 5th BPF, b) 6th BPF, c) 2210 Hz. The scale is in relation to the maximum value of SPL.

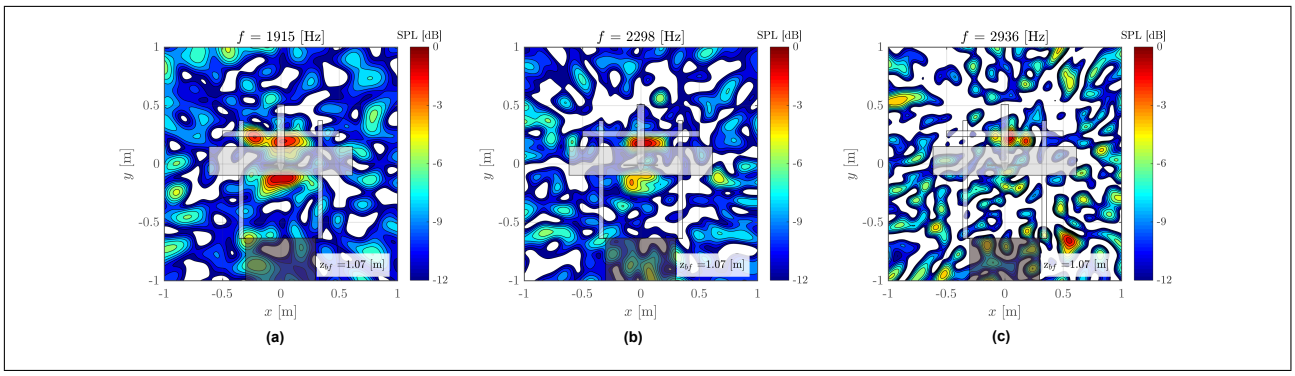

Figure 12. Beamforming for the propeller at the angular speed of BPF_3, for a frequency of: a) 5th BPF, b) 6th BPF, c) 2936 Hz. The scale is in relation to the maximum value of SPL.

References

[1] Y. Guo, M. Czech, and R. H. Thomas, "Open Rotor Noise Shielding by Blended-Wing-Body Aircraft," American Institute of Aeronautics and Astronautics, Jan. 2015.

[2] A. Synodinos, R. Self, and A. Torija, "Noise Assessment of Aircraft with Distributed Electric Propulsion Using a New Noise Estimation Framework," 2017.

[3] A. Agarwal, A. P. Dowling, H.-C. Shin, W. Graham, and S. Sefi, "Ray Tracing Approach to Calculate Acoustic Sheilding by a Flying Wing Airframe," *AIAA Journal*, vol. 45, pp. 1080–1090, May 2007.

[4] N. Turkdogru, K. Ahuja, and R. Gaeta, "Validity of the Point Source Assumption in Rotor Noise Measurements with Shielding," American Institute of Aeronautics and Astronautics, June 2010.

[5] Y. Guo, D. S. Pope, C. L. Burley, and R. H. Thomas, "Aircraft System Noise Shielding Prediction with a Kirchhoff Integral Method," American Institute of Aeronautics and Astronautics, June 2017.

[6] A. Vieira, M. Snellen, and D. G. Simons, "Assessing the shielding of engine noise by the wings for current aircraft using model predictions and measurements," *The Journal of the Acoustical Society of America*, vol. 143, no. 1, pp. 388–398, 2018.

[7] D. F. Colas and Z. Spakovszky, "A Turbomachinery Noise Shielding Framework Based on the Modified Theory of Physical Optics," American Institute of Aeronautics and Astronautics, May 2013.

[8] K. Miyamoto and E. Wolf, "Generalization of the Maggi-Rubinowicz theory of the boundary diffraction wave Part I," *JOSA*, vol. 52, no. 6, pp. 615–625, 1962.

[9] K. Miyamoto and E. Wolf, "Generalization of the Maggi-Rubinowicz theory of the boundary diffraction wave Part II," *JOSA*, vol. 52, no. 6, pp. 626–636, 1962.

[10] J. B. Keller, "Geometrical theory of diffraction," *JOSA*, vol. 52, no. 2, pp. 116–130, 1962.

[11] M. Born and E. Wolf, *Principles of optics, Electromagnetic theory of propagation, interference and diffraction of light*. Cambridge: Cambridge University Press, 1999.

[12] E. Sarradj, "Three-Dimensional Acoustic Source Mapping with Different Beamforming Steering Vector Formulations," *Advances in Acoustics and Vibration*, vol. 2012, pp. 1–12, 2012.

[13] S. Luesutthiviboon, A. Malgoezar, M. Snellen, and D. G. Simons, "Design of an optimized acoustic array for an open-jet anechoic wind tunnel with an application of advanced beamforming algorithms," (BeBeC Berlin 2018).

[14] D. W. Kurtz and J. E. Marte, "A review of aerodynamic noise from propellers, rotors, and lift fans," 1970.

[15] H. H. Hubbard, *Aeroacoustics of Flight Vehicles: Noise sources*, vol. 1. NASA Office of Management, Scientific and Technical Information Program, 1991.